Ultrafast dynamics of transition metal carbonyls.: II. Picosecond evaporation after photodissociation of Cr(CO)6·(CH3OH)n heteroclusters at 280 nm

ARTICLE *in* CHEMICAL PHYSICS · DECEMBER 1998

Impact Factor: 1.65 · DOI: 10.1016/S0301-0104(98)00348-6

ELSEVIER

Chemical Physics 239 (1998) 317–329

Chemical Physics

Ultrafast dynamics of transition metal carbonyls. II. Picosecond evaporation after photodissociation of $Cr(CO)_6 \cdot (CH_3OH)_n$ heteroclusters at 280 nm

Michael Gutmann *, Jörg M. Janello, Markus S. Dickebohm

Institut für Physikalische Chemie, Luxemburger Str. 116, D-50939 Köln, Germany

Received 8 April 1998

Abstract

Results of femtosecond pump–probe real-time studies on the evaporation dynamics following photodissociation of electronically excited $Cr(CO)_6 \cdot (CH_3OH)_n$ heteroclusters generated in a molecular beam are presented. The red part of the $^1T_{1u}$ metal-to-ligand charge transfer state at 280 nm is excited and the resulting photofragments are detected by multiphoton ionization. The time scale of the decarbonylation dynamics of $Cr(CO)_6$ within the clusters can be explained by a sequential mechanism when applying moderate pump intensities. Decarbonylation is found to be pulse-width limited and solvent evaporation from the solvated neutral photoproducts occurs on the picosecond time scale. Evidence for two different evaporation rates is provided, which by similarity to condensed-phase results from the literature can be interpreted in terms of vibrational energy transfer from low-frequency molecular modes to the solvent ($\sim$ 13 ps) and relaxation of high-frequency C–O stretch modes to anharmonically coupled low-frequency molecular modes ($\sim$ 100 ps). Solvated cluster species as well as coordinatively unsaturated carbonyls are stabilized by evaporation.

1. Introduction

Transition metal carbonyls serve as model systems for organometallic compounds, which are known to be of central importance for a number of catalytic processes in organic chemistry [1]. The coordinatively unsaturated fragments are believed to be the relevant reactive species in these processes. Thus investigation of the dynamics of coordinatively unsaturated transition metal carbonyls, especially the group-VIb hexacarbonyls and $Fe(CO)_5$ has been the subject of numerous studies, both experimental and theoretical, during the last two decades. In a recent contribution [2], henceforth referred to as Paper I, we presented a rather detailed account of important previous work, which we believe to be relevant for our experiments. We shall therefore only briefly mention some results from the literature here, which are especially important for the results presented in this contribution.

From spectroscopic investigations both in condensed phase and in gas phase [3–20] a so-called sequential model for the photodecarbonylation mechanism of $Cr(CO)_6$ after UV excitation has been put

* Corresponding author. E-mail: gutmann@fock.pc.uni-koeln.de

0301-0104/98/$ - see front matter
PII: S0301-0104(98)00348-6

forward. Within this model, the primary photofragment $Cr(CO)_5$ after excitation of $Cr(CO)_6$ into the $^1T_{1u}$ state is formed electronically excited in a square pyramid configuration,

$$Cr(CO)_6\left(^1T_{1u};O_h\right) \overset{-CO}{\rightarrow} Cr(CO)_5\left(^1E;C_{4v}\right). \quad (1)$$

In a next step, electronically excited $Cr(CO)_5$ relaxes to its equilibrium configuration, a trigonal bipyramid via

$$Cr(CO)_5\left(^1E;C_{4v}\right) \rightarrow Cr(CO)_5\left(^1E';D_{3h}\right), \quad (2)$$

from which it returns to the square pyramid configuration in its vibrationally excited electronic ground state due to a Jahn–Teller degeneracy in the D_{3h} geometry,

$$Cr(CO)_5\left(^1E';D_{3h}\right) \rightarrow Cr(CO)_5\left(^1A_1;C_{4v}\right). \quad (3)$$

In the gas phase the vibrational excess energy cannot be removed, so the ground state photofragment $Cr(CO)_5$ may further dissociate according to Eq. (4)

$$Cr(CO)_5\left(^1A_1;C_{4v}\right) \overset{-CO}{\rightarrow} Cr(CO)_4(C_{2v}). \quad (4)$$

Indeed, nanosecond studies confirmed $Cr(CO)_4$ to be the major metastable photofragment formed in the gas phase [14–16]. Recent femtosecond studies of the decarbonylation dynamics of $Cr(CO)_6$ in the gas phase could be interpreted within reaction steps (1)–(4) [2,21]. These studies showed that the decarbonylation dynamics occurs on a time scale of < 100 fs.

In condensed phase, excess vibrational energy is efficiently removed by the surrounding solvent atoms/molecules (S), and instead of reaction (4) solvent coordination takes place [22],

$$Cr(CO)_5 + S \rightarrow Cr(CO)_5 \cdot S. \quad (5)$$

Reformation of the (vibrationally excited) parent molecule via the cage effect is another pathway in condensed phase [22],

$$Cr(CO)_5 + CO \rightarrow Cr(CO)_6. \quad (6)$$

In both, gas phase and condensed phase, further absorption from the exciting laser pulse can lead to higher unsaturated photofragments down to $Cr(CO)_2$ within the sequential model [5].

Time-resolved studies employing femtosecond and picosecond lasers confirmed this picture of the condensed-phase dynamics [22–31]. In addition, time scales for vibrational relaxation could be determined. Joly and Nelson found that ejection of the first CO ligand from the electronically excited $Cr(CO)_6$ in various alcohols and in *n*-hexane is completed within 350 fs, coordination of the photofragment $Cr(CO)_5$ with methanol to form $Cr(CO)_5 \cdot (CH_3OH)$ occurs within 1.6 ps, and the time scale for vibrational relaxation of the complex $Cr(CO)_5 \cdot S$ is on the order of 50 ps, depending on the solvent used. Harris and co-workers observed dual cooling rates of $Cr(CO)_5 \cdot S$ with characteristic times of 18 and 150 ps, respectively, in their transient absorption experiments [27]. The slow component was assigned to relaxation of the high-frequency C–O stretch motion into lower-lying molecular modes. With transient IR spectroscopy Dougherty and Heilweil found similar cooling rates in *n*-hexane, 10 ps for relaxation of low-frequency vibrations and 160 ps for relaxation of the C–O stretch motion [31]. Fast geminate recombination according to step (6) has also been observed on a time scale of 150 fs in alkane solutions [28].

First spectroscopic studies on $Cr(CO)_6 \cdot (CH_3OH)_n$ van der Waals heteroclusters with nanosecond lasers were performed by Garvey and co-workers [32,33]. Their investigations were aimed at understanding the differences between gas- and condensed-phase decarbonylation of $Cr(CO)_6$. Fragment analysis after multiphoton ionization at 248 nm and in the region around 350 nm led to wavelength-dependent fragmentation patterns, which were attributed to the specific electronic state of the parent $Cr(CO)_6$ excited initially. The authors proposed solvated $Cr(CO)_4$ to be the primary metastable photofragment after excitation at 248 nm and $Cr(CO)_5$ after excitation at 350 nm.

Important theoretical work has been published [34–40], which helped to assign the electronic spectra [34] of $Cr(CO)_6$. Most importantly, recent calculations led to a reassignment of the lower-lying electronic states to metal-to-ligand charge transfer (MLCT) states as the ligand field (LF) states were calculated to be at much higher energies [38–40].

In Paper I we reported on real-time studies regarding the photodissociation dynamics of electronically excited ($^1T_{1u}$ at 280 nm) $Cr(CO)_6$ and $Cr(CO)_6 \cdot (CH_3OH)_n$ heteroclusters. It was found that the de-

carbonylation dynamics is much faster than the time resolution available (230 fs cross-correlation width) and that two fragmentation channels depending on pump laser intensity may be operative, the sequential one described above at lower intensities and a simultaneous one [41,42] where several CO ligands are lost at once. Both pathways were suggested to start from the primary photofragment $Cr(CO)_5$. Preliminary cluster studies presented in Paper I confirmed the existence of intensity-dependent dynamical pathways as the evaporation dynamics occurring on the picosecond time scale were found to exhibit different time scales depending on pump laser intensity.

In this contribution we shall present new results pertaining to the cluster dynamics of electronically excited ($^1T_{1u}$ at 280 nm) $Cr(CO)_6 \cdot (CH_3OH)_n$ heteroclusters on the picosecond time scale (up to 330 ps) in the lower pump intensity regime. We shall quantify relevant relaxation and evaporation times and compare our results with recent findings in condensed phase. In Section 2 we shall briefly describe our experimental setup used for obtaining our results, which will be presented and discussed in Section 3. Some concluding remarks will be given in Section 4.

2. Experimental

Our experimental setup has been described in detail in Paper I. Briefly, we used a femtosecond Ti:sapphire amplifier (BMI, Alpha 10 series) consisting of a reflective stretcher, a Nd:YAG laser (532 nm) pumped regenerative amplifier, a four-pass bowtie amplifier pumped by the same Nd:YAG laser (532 nm), and a two-grating compressor to amplify pulses of an argon ion laser (Coherent, Innova 310) pumped Ti:sapphire oscillator (Coherent, Mira Basic). The amplified output pulses centered at 805 nm have an energy of ~ 17 mJ and a pulse duration of $\sim 80-100$ fs at a repetition rate of 10 Hz. After frequency doubling in a 0.5 mm thick BBO I crystal pulses centered at ~ 402.5 nm with energies of ~ 7 mJ are obtained, which serve as pump pulses for two simultaneously pumped home-built two-stage white-light seeded optical parametric amplifiers (OPAs). The laser system is schematically depicted in Fig. 1. For the one-color experiments presented here, only one of the two OPAs was used, which was tuned to a center wavelength of 560 nm. The output (pulse energy: ~ 50 μJ, intensity autocorrelation width: < 300 fs) was split into two beams by a beamsplit-

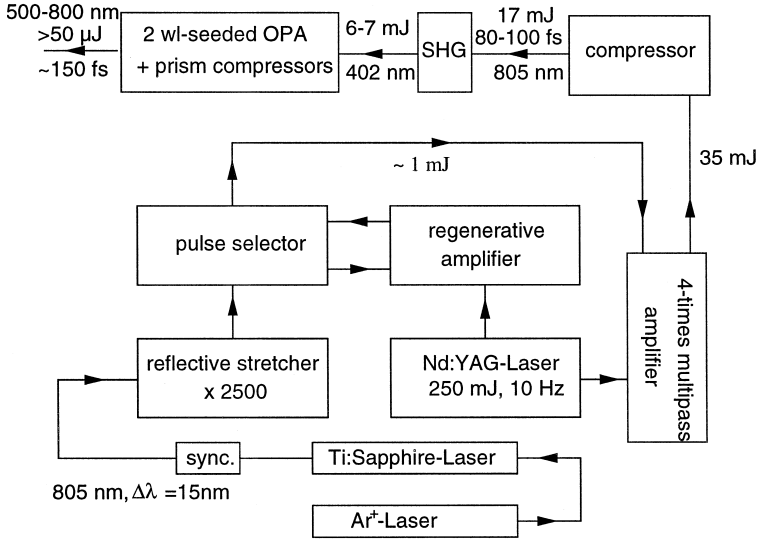

Fig. 1. Schematic of the laser setup.

ter. The two beams were delayed with respect to each other by a Michelson interferometer type setup where the pump beam was sent down a fixed delay stage and the probe beam was sent down a variable delay stage (Aerotech, ATS 0230 with stepper motor). Both beams were recombined on a second beamsplitter and sent through a 0.2 mm thick BBO I crystal to yield femtosecond pump and probe pulses centered at 280 nm, which were focused into the molecular beam. Typical laser intensity in the overlap region of pump and probe pulses was estimated to be 10^{10}–10^{11} W cm^{-2}. Thus nonperturbative effects which become important at higher laser intensities (intensities above 10^{13} W cm^{-2} [43]) do not play a major role in the experiments discussed here.

For preparation of the $Cr(CO)_6 \cdot (CH_3OH)_n$ heteroclusters we used the molecular beam apparatus shown in Fig. 2, which consists of two differentially pumped chambers, a main chamber housing the pulsed solenoid nozzle (General Valve, Series 9 with home-built conical orifice of 200 μm diameter driven by a home-built triggering and driver assembly yielding clean gas pulses of ~100 μs width), which is separated from the buffer chamber by a rhodium plated nickel skimmer (Beam Dynamics) of 1.5 mm diameter. The buffer chamber houses a home-built linear time-of-flight (TOF) mass spectrometer of Wiley-McLaren type [44] with a multichannel plate detector (Hamamatsu, F1552-29S).

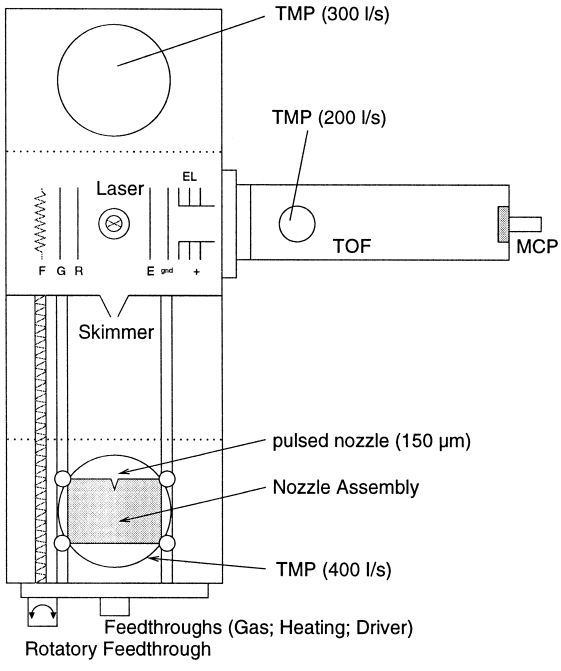

Fig. 2. Schematic of the molecular beam apparatus (TMP = turbomolecular pump; F = filament; G = grid; R = repeller; E = extractor; gnd = ground; EL = Einzel lens assembly; TOF = time-of-flight mass spectrometer; MCP = multichannel plate).

$Cr(CO)_6 \cdot (CH_3OH)_n$ heteroclusters were produced by bubbling neon gas (Linde, 99.995%) through a reservoir of methanol (Merck, 99.9%) and seeding the beam at backing pressures of typically 4 bar with heated (~375 K) $Cr(CO)_6$ (Aldrich, 99%, used as received). A typical nozzle to skimmer distance of $x/d \approx 100$ was kept. The nozzle and the laser system were triggered externally at 10 Hz and synchronized such that gas and laser pulses overlapped in time in a region where cluster formation could be observed. With the nozzle on, the pressure in the main chamber was below 10^{-4} mbar and in the TOF tube it was below 4×10^{-7} mbar.

Experiments were carried out such that the femtosecond pump pulse at 280 nm excited the red part of the $^1T_{1u}$ state of $Cr(CO)_6$, from which the decarbonylation dynamics started. Care was taken that the pump pulse did not by itself produce any measurable ion signal, so the dynamical processes observed were taking place in the neutral manifold. The delayed strong probe pulse at 280 nm ionized the nascent photofragments by multiphoton ionization (MPI). The term strong in this context is used in a loose fashion to distinguish the pump pulse which was not able to produce any ions by itself from the probe pulse which gave rise to some background ion signal [1]. The ion signal after preamplification by a home-built amplifier was fed into a digital signal analyzer (Tektronix, DSA 601) where the resulting mass spectra were averaged for a number of preset shots (usually 100). The averaged mass spectra together with the respective position of the delay stage were stored and sent to a PC after each scan. A number of scans (38 in the time range 0–6.5 ps and 18 in the

[1] We thank one of the referees for pointing out that in the strong laser field community a strong femtosecond laser pulse refers to a pulse of such an intensity that a perturbation theoretical approach is no longer applicable. This is by no means implied by our usage of the term strong; here we deal with intensities of much less than 10^{12} W/cm^2.

time range up to 330 ps) was averaged, and the transients for each mass peak of interest was obtained by integrating the corresponding peak areas for each delay position. Data analysis and fitting were performed on a DEC Alpha workstation.

3. Results and discussion

3.1. Femtosecond mass spectra

In Fig. 3 a femtosecond mass spectrum of $Cr(CO)_6 \cdot (CH_3OH)_n$ heteroclusters obtained by MPI at 280 nm is shown.

The spectrum is dominated by the bare Cr^+ ion signal, the unsolvated coordinatively unsaturated ions $Cr(CO)^+$, $Cr(CO)_2^+$, $Cr(CO)_3^+$, the parent ion, and solvated Cr^+ ions. Coordinatively unsaturated solvated photofragment ions $CrL_n^+S_m$ (L = CO, S = CH_3OH) are not observed for small $m + n < 4$; only at higher solvation there exist mass peaks, which can be assigned to such species. This observation is basically in accord with the moderate intensity (10^7–10^8 W cm^{-2}) nanosecond MPI mass spectra obtained by Peifer and Garvey [33] at 248 nm ($^1T_{1u}$ MLCT state). We, too, observe the homogeneous solvent cluster ions S_mH^+ and a pronounced sequence $Cr^+ \cdot S_m$. Ion peaks corresponding to $Cr(CO)^+ \cdot S_m$ appear at $m \geq 4$ in accord with Ref. [32]. $Cr(CO)_2^+ \cdot S_5$ can also be tentatively assigned. In addition, we observe bi- and trinuclear homogeneous metal cluster ions and their carbonyl complexes (Cr_2^+, Cr_3^+, $Cr_2(CO)^+$, $Cr_2(CO)_3^+$) which may be indicative of homogeneous cluster reactions. We obtained preliminary experimental results showing picosecond dynamics at some of these homogeneous metal peaks which clearly show that these species are formed by intra-cluster reaction in the neutral manifold and not by ion-molecule collisions. Further investigations on the homogeneous cluster dynamics are underway in our laboratory.

It should be noted that a number of mass peaks cannot be unambiguously assigned due to isobaric interferences, for example $Cr(CO)_3$ and $Cr_2 \cdot (CH_3OH)$, $Cr(CO)_3 \cdot (CH_3OH)_n$ and $Cr_2 \cdot (CH_3OH)_{n+1}$. By comparing with experiments where the clustering conditions were different and less homogeneous metal species were present, we can at least assign some of the ambiguous mass peaks with reasonable confidence, however, experiments with deuterated methanol as a solvent are underway to clarify the assignments. In the following we shall only discuss dynamics at mass positions were the assignments were unique.

The fact that we observe strong signals from unsolvated coordinatively unsaturated carbonyls and

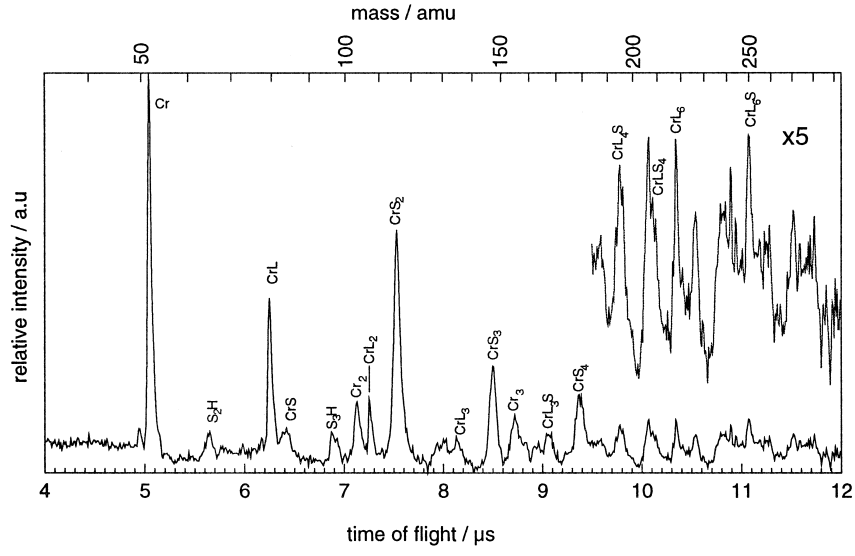

Fig. 3. Femtosecond TOF mass spectrum of $Cr(CO)_6 \cdot (CH_3OH)_n$ heteroclusters obtained by MPI (L = CO; S = CH_3OH).

only small signals from the corresponding solvated ones can be explained considering the ultrafast decarbonylation dynamics. First, the molecular beam contains unsolvated $Cr(CO)_6$ molecules which after ultrafast decarbonylation, as described in Paper I, lead to coordinatively unsaturated carbonyl ions and Cr^+ when probed by the second laser pulse. In addition, the solvent-to-ion binding energy will be much larger than the solvent binding energy in the neutral, i.e., the ionization energy of the initially formed neutral photofragment will decrease with increasing solvation. Thus solvated ions produced by the probe pulse will contain much more excess energy than the corresponding unsolvated ions, which leads to a higher fragmentation probability in the ion channel yielding unsolvated unsaturated carbonyl ions and solvated chromium ions. Tuning the probe laser wavelength into the red will be a check on this hypothesis.

In the following we shall discuss the picosecond evaporation dynamics obtained at a number of selected mass peaks in more detail.

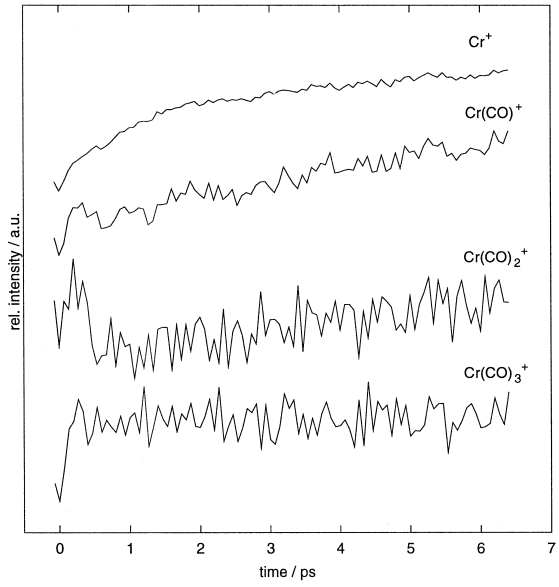

Fig. 4. Cluster transients obtained at mass peaks of Cr^+ and $Cr(CO)_n^+$ $(n = 1–3)$ for the first 6.5 ps. Signal at negative time delays is due to exchange of pump and probe pulses in the one-color experiments.

3.2. Cluster dynamics

In Paper I we gave a preliminary account on the solvation dynamics of $Cr(CO)_6 \cdot (CH_3OH)_n$ heteroclusters after exciting $Cr(CO)_6$ into the electronic $^1T_{1u}$ state at 280 nm. It was found that the cluster dynamics occurs on the picosecond time scale, i.e., ultrafast decarbonylation is completed before evaporation sets in. By following the dynamics for a rather short time (< 30 ps) it was shown that the evaporation rate depends strongly on the pump intensity. Using a weak pump pulse and a stronger probe pulse (weak pump regime) evaporation was found to be significantly slower than by using the stronger pulse as pump and the weak one as probe. These findings were taken as evidence for different decarbonylation pathways being operative, the consecutive pathway discussed in Section 1 dominating in the weak pump regime and a simultaneous pathway dominating in the strong pump regime. The results presented and discussed in this section all belong to the weak pump regime. Here, evaporation time scales will be defined and discussed with respect to literature on the cooling dynamics observed in solution.

In Fig. 4 transients obtained at mass peaks Cr^+, $Cr(CO)^+$, $Cr(CO)_2^+$ and $Cr(CO)_3^+$ for the first 6.5 ps are shown. Transients obtained at masses $Cr(CO)^+$ and $Cr(CO)_2^+$ show more or less pronounced transient peaks close to zero delay. These peaks can be attributed to the decarbonylation dynamics of bare $Cr(CO)_6$ and were interpreted in Paper I as being due to the transition of the primary electronically excited photofragment $Cr(CO)_5$ from the square pyramid towards the trigonal bipyramid ending up in the vibrationally excited electronic ground state of the square pyramid configuration (see Eqs. (2) and (3)). In opposite to the bare $Cr(CO)_6$ dynamics, however, all transients except the one taken at the $Cr(CO)_3^+$ peak position show a rise on the picosecond time scale. The fact that the $Cr(CO)_3^+$ transient behaves differently may be due to isobaric interference from $Cr_2^+ \cdot CH_3OH$.

In order to obtain a hint to possible solvated photofragments from which solvent evaporation may occur, a discussion of multiphoton fragmentation pathways is in order. Since the pump laser was attenuated to a level were ion signal by the pump alone could hardly be detected, fragmentation induced by pump photons can only occur in the neutral. Excitation of $Cr(CO)_6$ thus is only possible by a

single pump photon at 280 nm since absorption of a second pump photon leads into the ion channel as can be seen from the energetics shown in Fig. 5 and listed in Table 1.

The primary photoproduct $Cr(CO)_5$ (^1E) excited at $\sim$16000–20000 cm^{-1} above the ground state [4] can be two-photon ionized by the probe pulse and can thus lead to ions from $Cr(CO)_5^+$ down to $Cr(CO)^+$. Of these only $Cr(CO)_n^+$ ($n = 1$–3) can clearly be observed in the mass spectra (see Fig. 3). The primary photofragment $Cr(CO)_5$ can in principle absorb another pump photon leading to a highly excited state 51000–55000 cm^{-1} above the ground state, from which fragmentation down to bare Cr is possible. Since $Cr(CO)_5$ appears to be extremely short-lived (we observed pulse-width limited transient peaks in Paper I and in a recent publication [49] on the fragmentation dynamics of $Fe(CO)_5$ it was shown that the rise time of the primary photofragment could not be fitted using pulses of < 100 fs), such a pathway may become important at high laser intensities [2,41,42]. As discussed in Section 1, the primary photofragment $Cr(CO)_5$ can further dissociate to $Cr(CO)_4$ (see Eq. (4)). Two-photon ionization of the hot fragment $Cr(CO)_4$ at 280 nm cannot produce the Cr^+ ions observed as can be deduced from the energetics. Due to the fact that the probe pulse was able to produce some background ion signal from the sample, three-photon absorption from the probe pulse is possible. Thus solvated and unsolvated Cr^+ ions may derive from neutral solvated $Cr(CO)_4$ photofragments. In addition, some of these ions may also be formed from nascent $Cr(CO)_5$ after absorption of an additional pump photon, leading to further fragmentation in the neutral manifold and subsequent two-photon ionization by the probe pulse. Possible products in the neutral are thus either one-photon products (most likely solvated $Cr(CO)_4$) or two-photon products (most likely solvated smaller fragments $Cr(CO)_n$). Three-photon products in the neutral can only arise from two-photon products which after absorption of an additional pump photon must have lost large amounts of excess energy in order not to be ionized directly. This does not appear to be very probable during the pulse width of the pump laser ($\sim$ 150 fs as obtained from autocorrelation measurements).

Ionization of the neutral solvated photoproducts by the probe pulse occurs via a three-photon process or a two-photon process. It is possible that additional probe photons are absorbed in the ion channel; however, since slight attenuation of the probe pulse did not lead to significant changes in the mass spectra

Table 1
Bond dissociation energies (BDEs) of neutral and ionic $Cr(CO)_6$

Cr–CO bond number	BDE (neutral) (cm^{-1})	BDE (ion)[a] (cm^{-1}) (ionization potential: 8.10 ± 0.01 eV)[a]
1	12950 ± 1750[b]	9600 ± 160
2	8750 ± 1750[b]	4520 ± 240
3	12250 ± 5250[c]	6210 ± 320
4	6650 ± 5250[d]	5240 ± 400
5	6650 ± 5250[d]	15490 ± 480
6	6650 ± 5250[d]	7500 ± 480

[a] Taken from Ref. [46].
[b] Taken from Ref. [47].
[c] Taken from Ref. [48].
[d] Averaged BDE's according to Ref. [32].

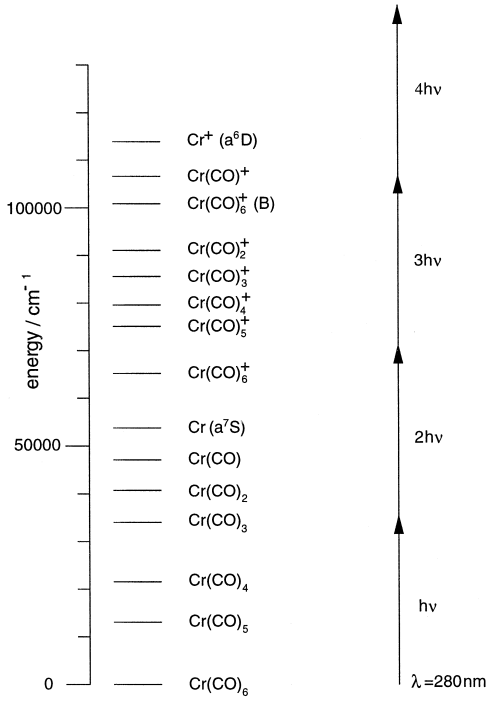

Fig. 5. Energetics of neutral and ionic $Cr(CO)_n$ ($n = 0$–6) species derived from the entries of Table 1. The position of the ionic B state was taken from Ref. [45].

observed, we may assume three- and two-photon fragment ionization. Attempts to separate the two-photon probe channel from any multiphoton channels by attenuating our lasers were not successful due to very low signal strengths. Even at rather low intensities the Cr^+ mass peak was observed. If this picture is true and remains valid for the corresponding solvent heteroclusters, transients derived from Cr^+ and solvated Cr^+ mass peaks should mainly be a signature of the dynamics of coordinatively unsaturated (solvated) $Cr(CO)_4$ in the neutral manifold. As the cluster dynamics observed takes place on the picosecond time scale, the complete femtosecond decarbonylation reaction is over before evaporation can be observed. With these considerations in mind, we propose that the solvation dynamics obtained from transients at $Cr^+ \cdot S_n$ mass peaks, to be discussed in the following, derives from solvated coordinatively unsaturated neutral $Cr(CO)_4$.

In contrast to the dynamics observed for unsolvated $Cr(CO)_6$ (see Paper I) all transients shown in Fig. 4 except the one taken at the $Cr(CO)_3^+$ mass peak exhibit a pronounced rise starting after ~ 500 fs and do not level off after 6.5 ps. The rise of all these transients continues for longer times (not shown here). These species must therefore derive from solvated precursors, which have lost their solvent molecules either in the neutral or in the ionic manifold. Coordinatively unsaturated carbonyls are stabilized by excess energy transfer to solvent molecules, which evaporate from the cluster. We also observed a slow rise of the unsolvated parent ion $Cr(CO)_6^+$ due to clustering, which has yet to be explained, possibly by the cage effect.

In Fig. 6 transients measured at masses of the solvated cluster ions $Cr^+ \cdot S_n$ ($n = 1$–4) on the same time scale are shown. It can be seen that the rise times decrease considerably with increasing n. The $Cr^+ \cdot (CH_3OH)$ transient does not level off after 6.5 ps; fitting after convolution of a gaussian of experimental intensity autocorrelation width with a double-exponential rise leads to rise times of 140 fs and 2.0 ps, respectively. The initial rise times of the $Cr^+ \cdot S_n$ ($n = 2$–4) transients were obtained by fitting after convoluting a gaussian of experimental intensity autocorrelation width with a single-exponential rise and a single-exponential decay in the time range shown in Fig. 6. The decay time was kept

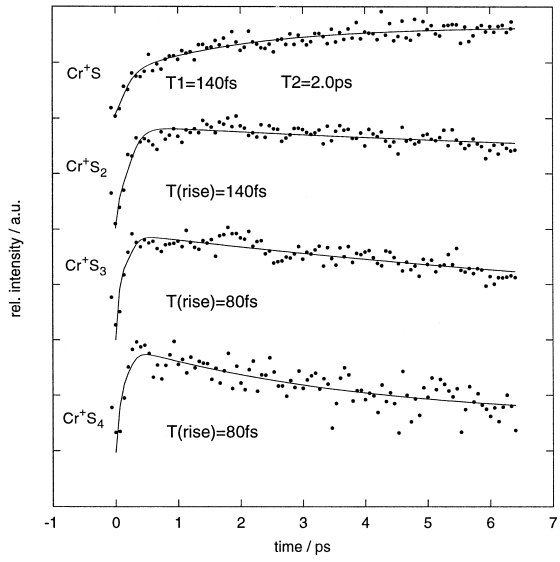

Fig. 6. Cluster transients obtained at mass peaks of $Cr^+ \cdot S_n$ ($n = 1$–4) ($S = CH_3OH$). Rise times obtained after convolution with a gaussian of intensity autocorrelation width are indicated in the figure ($T1$, $T2$ for $Cr^+ S$, T(rise) for $Cr^+ \cdot S_n$ ($n = 2$–4), see text for details).

at the value of the shorter of the two decay times obtained from the corresponding transients on the longer time scale (vide infra). By that procedure we obtained initial rise times of 140 fs ($Cr^+ \cdot (CH_3OH)_2$), 80 fs ($Cr^+ \cdot (CH_3OH)_3$), and 80 fs ($Cr^+ \cdot (CH_3OH)_4$). Especially the latter two rise times have to be interpreted with caution due to the experimental time resolution and the signal to noise ratio observed. However, we may conclude that the time of formation of the solvated photofragments in the neutral, which give rise to the observed transients decreases with increasing cluster size. The solvated neutral fragments leading to the $Cr^+ \cdot (CH_3OH)$ signal can obviously be stabilized on the picosecond time scale. As the decay times of the $Cr^+ \cdot S_n$ transients are much longer than the rise times (vide infra), solvent molecules are not lost consecutively, i.e., in going from n to $n-1$. It appears to be much more likely that after the decarbonylation reaction in the clusters part of the remaining excess energy is used to dissociate a number of solvent molecules very rapidly (on the femtosecond time scale), after which evaporation on the picosecond time scale takes place. Thus two kinds of solvent loss can be distinguished, an impul-

sive one connected to the decarbonylation and an evaporative one connected to vibrational energy transfer.

Fig. 7 shows transients obtained for Cr^+ and $Cr(CO)^+$ on a longer time scale. Shown are also fits to a double-exponential rise starting after 600 fs together with the corresponding residuals. It is clearly seen that the fit represents the experimental data quite well, indicating that the cluster dynamics involves at least two different processes, one on a time scale of ~ 7 ps and the other on a time scale of ~ 90 ps.

Fig. 8 shows a transient obtained for $Cr^+ \cdot (CH_3OH)_2$ together with fits to a single-exponential decay (a) and a double-exponential decay (b) and the respective residuals. The asymptotic value of the fits was fixed at the end of the transient, all other parameters were used as fit parameters.

From the fits and the residuals it is obvious that a single-exponential decay does not fit the data of the initial part of the decay satisfactorily, whereas the double-exponential decay represents the experimental data quite well. Thus there is evidence that the cluster dynamics involves at least two dynamical channels on the picosecond time scale. In Fig. 9 transients for $Cr^+(CH_3OH)_3$ and $Cr^+(CH_3OH)_4$ together with fits to a double-exponential decay and the corresponding residuals are shown. Again, the asymptotic value of the fits was fixed at the end of the transient, all other parameters were used as fit parameters.

All transients obtained for the solvated chromium ion exhibit similar time scales, a short one of ~ 13 ps and a long one of ~ 100 ps. None of these decay times matches the rise times of any $Cr^+ \cdot S_n$ transient with lower n. As the picosecond rise of the Cr^+ and $Cr(CO)^+$ transients after a fast initial rise exhibit comparable time scales it is quite likely that they are dynamically linked to the decay observed for the solvated Cr^+ transients. Assuming that the neutral

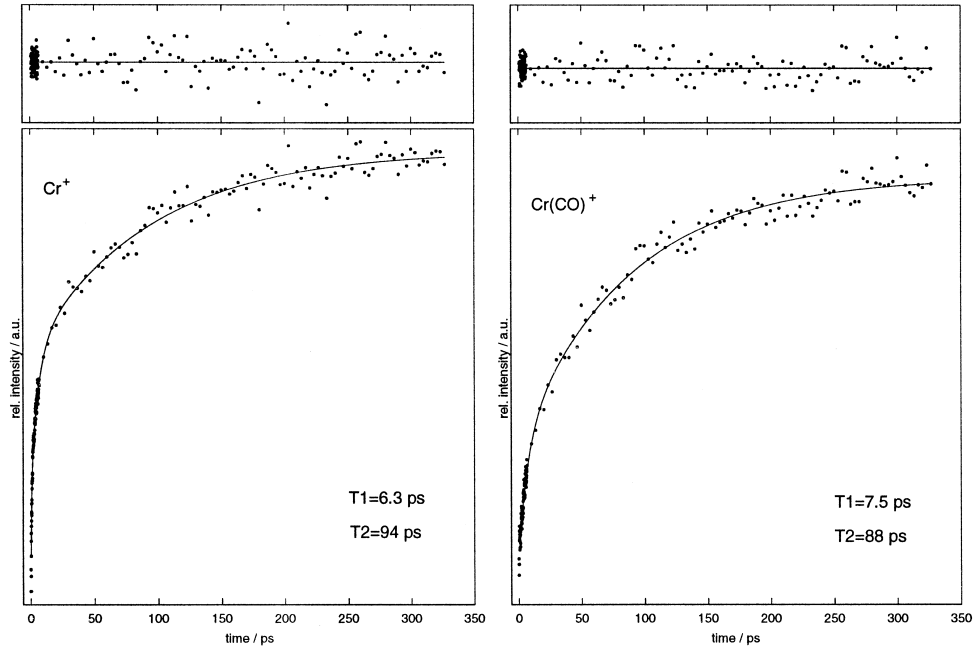

Fig. 7. Cluster transients obtained at mass peaks Cr^+ and $CrCO^+$ on a longer time scale. Shown are fits (solid lines) to a double-exponential rise (starting at 600 fs), and the characteristic rise times $T1$ and $T2$ are indicated. Residuals are shown in the upper parts of the figures with the solid line indicating zero deviation.

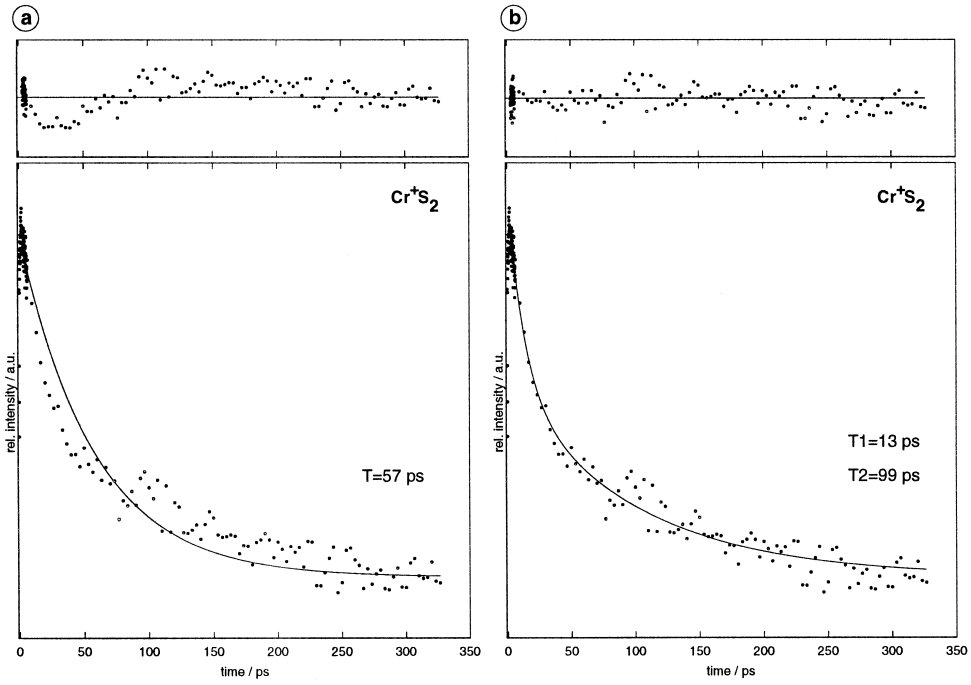

Fig. 8. Cluster transient obtained at mass peak of $Cr^+ \cdot S_2$ ($S = CH_3OH$) on a longer time scale. A comparison between fits (solid lines) to a single-exponential decay (a) and to a double-exponential decay (b) starting at signal maximum is shown, and the characteristic decay times (T, $T1$, $T2$) are indicated. Residuals are shown in the upper parts of (a) and (b) with the solid line indicating zero deviation.

precursor is solvated $Cr(CO)_4$ we propose that after an initial loss of solvent molecules, which is connected to the decarbonylation process, evaporation down to bare $Cr(CO)_4$ and less solvated $Cr(CO)_4$ takes place on the picosecond time scale. Upon ionization these photofragments yield bare Cr^+ and $Cr(CO)^+$ ions as well as $Cr^+ \cdot (CH_3OH)_n$ cluster ions.

The question to be answered then is: How can we explain the two different time scales observed in the picosecond evaporation dynamics? If we compare our results with the condensed-phase real-time experiments of Harris and co-workers and of Dougherty and Heilweil [27,31], a possible explanation is evaporation due to vibrational cooling of different types of excited molecular vibrational modes. With picosecond pump–probe transient-absorption spectroscopy, Harris and co-workers studied the photodissociation of a CO ligand from electronically excited (295 nm) $Cr(CO)_6$ in cyclohexane as a solvent (S). From the spectral evolution of the absorption in time, the authors determined two vibrational cooling times for the species $Cr(CO)_5 \cdot S$, a short one of 18 ps and a long one of 150 ps. Referring to transient Raman work [50] and earlier results by Heilweil and co-workers [51], Harris and co-workers assigned the slow component to vibrational relaxation of the C–O stretch modes to low-frequency molecular modes. Transient IR absorption experiments using broadband IR pulses of 300 fs pulse duration after UV excitation of $Cr(CO)_6$ in *n*-hexane as a solvent (S) at 289 nm (150 fs pulse width) were performed to follow relaxation of the excited C–O stretch mode of photofragment $Cr(CO)_5 \cdot S$ [31]. Transient narrowing and blue shift of the absorption peak within ~ 10 ps was interpreted in terms of vibrational relaxation of excited low-frequency molecular modes. The vibrationally excited C–O stretches were found to relax within ~ 160 ps via anharmonic coupling to low-frequency modes.

Even though the evaporation dynamics we observe originates from a different photofragment (most

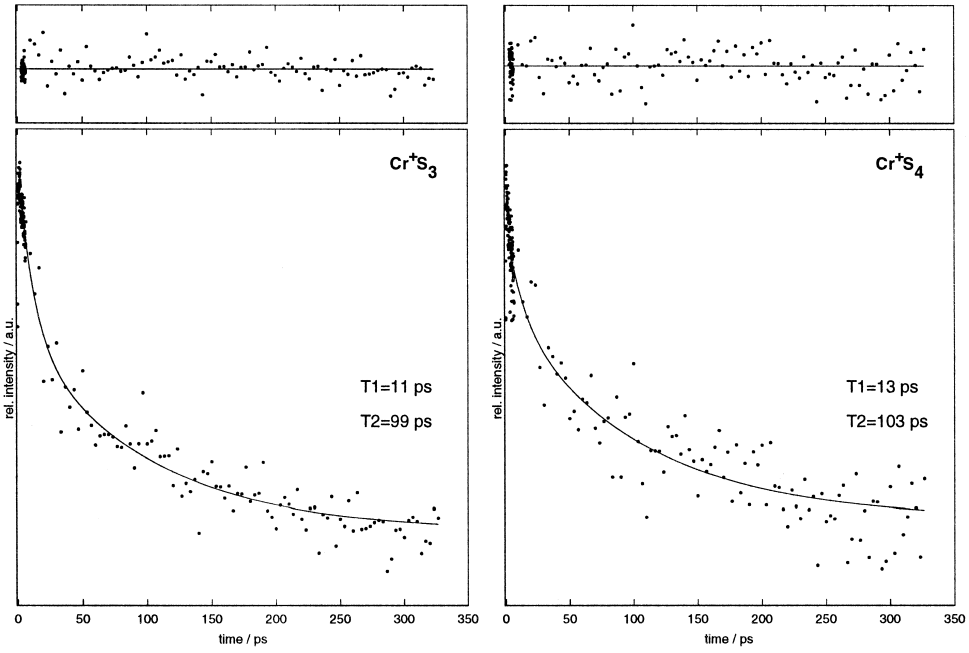

Fig. 9. Cluster transients obtained at mass peaks $Cr^+ \cdot S_3$ and $Cr^+ \cdot S_4$ ($S = CH_3OH$) on a longer time scale. Shown are fits (solid lines) to a double-exponential decay starting at signal maximum, and the characteristic rise times $T1$ and $T2$ are indicated. Residuals are shown in the upper part of the figure with the solid line indicating zero deviation.

likely solvated $Cr(CO)_4$, vide supra), the fact that we observe a bimodal behavior with time scales comparable to those observed in solution studies leads us to propose a similar mechanism of cluster evaporation. The shorter time (7–13 ps) observed in our experiments may then be due to vibrational relaxation of excited low-frequency molecular modes by transferring kinetic energy to the van der Waals modes, leading to bond rupture of the solvent-to-photofragment van der Waals bond. Similarly, the longer time (90–100 ps) can be explained by relaxation of excited high-frequency C–O stretch modes to low-frequency molecular modes via anharmonic coupling, subsequent transfer of kinetic energy to the van der Waals cluster modes followed by van der Waals bond breakage. The bottleneck of this second evaporation channel will then be intramolecular vibrational energy redistribution (IVR) of C–O stretch excitation towards low-frequency accepting modes before transfer of vibrational energy to the van der Waals modes takes place. This interpretation is similar to what Bernstein discussed as IVR preceding VP (vibrational predissociation) [52].

We performed additional experiments (not shown here) at a different pump wavelength (centered at 262.5 nm) in order to study the influence of excess energy on the evaporation dynamics. The behavior of all transients observed was very similar to the ones presented here and preliminary rise and decay times obtained are of the same order of magnitude as those presented here. Again, bimodal behavior can be observed; however, the longer decay time appears to become smaller due to deposited excess energy.

4. Conclusions

From the results presented in this contribution we may conclude that both gas-phase dynamics and condensed-phase dynamics are observable in the electronically excited $Cr(CO)_6 \cdot (CH_3OH)_n$ heteroclusters. Ultrafast decarbonylation appears to follow the consecutive gas-phase mechanism discussed in Section 1. Under our experimental conditions we could not yet produce significant amounts of clusters

large enough to trap the solvated primary photoproduct $Cr(CO)_5$. The fact that we observe mass peaks corresponding to $Cr(CO)_3^+ \cdot (CH_3OH)_n$ and $Cr(CO)_4^+ \cdot (CH_3OH)_n$ may point to such a possibility. Further experiments directed at producing larger clusters in higher quantities are necessary and will be performed in our laboratory. In contrast to the experiments on bare $Cr(CO)_6$ discussed in Paper I we do, however, observe a rise of the $Cr(CO)_2^+$ transient on the picosecond time scale, which can be taken as evidence for stabilization of coordinatively unsaturated carbonyls by loss of excess energy via evaporation of solvent molecules.

From the rise and decay times of the solvated cluster transients two different mechanisms of solvent loss could be derived, an impulsive one on the femtosecond time scale, connected directly to the decarbonylation dynamics, and an evaporative one on the picosecond time scale. Analysis of the evaporation dynamics of a photoproduct, which upon probe ionization leads to unsolvated and solvated Cr^+ ions and to unsolvated $Cr(CO)^+$ ions (most likely solvated coordinatively unsaturated $Cr(CO)_4$) on the picosecond time scale clearly revealed two different evaporation times which are very close in magnitude to vibrational cooling times observed in condensed-phase studies. The shorter time (7 ps for the unsolvated transients and ~ 13 ps for the solvated transients) was attributed to vibrational relaxation from excited molecular low-frequency modes to the surrounding solvent molecules, which then dissociate from the cluster. The longer time (90 ps for the unsolvated transients and ~ 100 ps for the solvated transients) was interpreted in terms of relaxation from high-frequency C–O stretches to low-frequency molecular modes via anharmonic coupling, followed by vibrational energy transfer to the solvent molecules, which then evaporate from the cluster. Further experiments are planned in order to test this interpretation. Different solvent molecules should yield different evaporation times; perdeuterated methanol, e.g., will provide a different set of low-frequency modes as accepting bath modes without changing the geometry of the cluster with respect to methanol as a solvent. The influence of the excess energy in the ion channel on the cluster ion distribution will provide invaluable hints to the actual neutral photoproduct from which evaporation is observed. This influence can be studied by varying the probe laser wavelength. Varying the pump laser wavelength within the $^1T_{1u}$ state will provide information on the dependence of the dynamics on excess energy in the neutral manifold.

Our aim in this series of experiments is to understand the difference in dynamics between the decarbonylation mechanism in gas phase and condensed phase for a number of organometallic compounds and solvents. We hope that this contribution provides a step towards reaching that goal.

Acknowledgements

Financial support by the Deutsche Forschungsgemeinschaft (grant Gu 280/3) via the Schwerpunktprogramm ''Molekulare Cluster'' is gratefully acknowledged. One of us (MSD) wishes to thank the Fonds der Chemischen Industrie for a graduate fellowship. We also thank Professor G. Hohlneicher for continuous support.

References

[1] A. Yamamoto, Organotransition Metal Chemistry, Fundamental Concepts and Applications, Wiley, New York, 1986.
[2] M. Gutmann, J.M. Janello, M.S. Dickebohm, M. Großekathöfer, J. Lindener-Roenneke, J. Phys. Chem. A 102 (1998) 4138, in the present paper referred to as Paper I.
[3] J. Burdett, R.N. Perutz, M. Poliakoff, J.J. Turner, J. Chem. Soc., Chem. Commun. (1975) 157.
[4] R.N. Perutz, J.J. Turner, J. Am. Chem. Soc. 97 (1975) 4791.
[5] R.N. Perutz, J.J. Turner, J. Am. Chem. Soc. 97 (1975) 4800.
[6] R.N. Perutz, J.J. Turner, Inorg. Chem. 14 (1975) 262.
[7] J. Burdett, M.A. Graham, R.N. Perutz, M. Poliakoff, J.A. Rest, J.J. Turner, A.F. Turner, J. Am. Chem. Soc. 97 (1975) 4805.
[8] J. Burdett, J.M. Grzybowski, R.N. Perutz, M. Poliakoff, J.J. Turner, R.F. Turner, Inorg. Chem. 17 (1978) 147.
[9] J.J. Turner, J.K. Burdett, R.N. Perutz, M. Poliakoff, Pure Appl. Chem. 49 (1977) 271.
[10] J.M. Kelly, H. Hermann, E. Koerner von Gustorf, J. Chem. Soc., Chem. Commun. (1973) 105.
[11] J.M. Kelly, D.V. Bent, H. Hermann, D. Schulte-Frohlinde, E. Koerner von Gustorf, J. Organomet. Chem. 69 (1974) 259.
[12] G. Nathanson, B. Gitlin, A.M. Rosan, J.T. Yardley, J. Chem. Phys. 74 (1981) 361.
[13] J.T. Yardley, B. Gitlin, G. Nathanson, A.M. Rosan, J. Chem. Phys. 74 (1981) 370.
[14] W. Tumas, B. Gitlin, A.M. Rosan, J.T. Yardley, J. Am. Chem. Soc. 104 (1982) 55.

[15] T.R. Fletcher, R.N. Rosenfeld, J.T. Yardley, J. Am. Chem. Soc. 107 (1985) 2203.
[16] G.W. Tyndall, R.L. Jackson, J. Chem. Phys. 91 (1989) 2881.
[17] W.H. Breckenridge, G.M. Stewart, J. Am. Chem. Soc. 108 (1986) 364.
[18] T.A. Seder, S.P. Church, E. Weitz, J. Am. Chem. Soc. 108 (1986) 4721.
[19] E. Weitz, J. Phys. Chem. 91 (1987) 3945.
[20] J.R. Wells, E. Weitz, J. Am. Chem. Soc. 114 (1992) 2783.
[21] S.A. Trushin, W. Fuß, W.E. Schmid, K.L. Kompa, J. Phys. Chem. A 102 (1998) 4129.
[22] J.A. Welch, K.S. Peters, V. Vaida, J. Phys. Chem. 86 (1992) 1941.
[23] J.D. Simon, K.S. Peters, Chem. Phys. Lett. 98 (1983) 53.
[24] J.D. Simon, X. Xie, J. Phys. Chem. 90 (1986) 6751.
[25] J.D. Simon, X. Xie, J. Phys. Chem. 91 (1987) 5538.
[26] M. Lee, C.B. Harris, J. Am. Chem. Soc. 111 (1989) 8963.
[27] J.C. King, J.Z. Zhang, B.J. Schwartz, C.B. Harris, J. Chem. Phys. 99 (1993) 7595.
[28] T. Lian, S.E. Bromberg, M.C. Asplund, H. Yang, C.B. Harris, J. Phys. Chem. 100 (1996) 11994.
[29] A.G. Joly, K.A. Nelson, J. Phys. Chem. 93 (1989) 2876.
[30] A.G. Joly, K.A. Nelson, Chem. Phys. 152 (1991) 69.
[31] T.P. Dougherty, E.J. Heilweil, Chem. Phys. Lett. 227 (1994) 19.
[32] W.R. Peifer, J.F. Garvey, J. Chem. Phys. 94 (1991) 4821.
[33] W.R. Peifer, J.F. Garvey, J. Phys. Chem. 95 (1991) 1177.
[34] N.A. Beach, H.B. Gray, J. Am. Chem. Soc. 90 (1968) 5713.
[35] P.J. Hay, J. Am. Chem. Soc. 100 (1978) 2411.
[36] J. Li, G. Schreckenbach, T. Ziegler, J. Phys. Chem. 98 (1994) 4838.
[37] L.A. Barnes, B. Liu, R. Lindh, J. Chem. Phys. 98 (1993) 3978.
[38] B.J. Persson, B.O. Roos, J. Chem. Phys. 101 (1994) 6810.
[39] K. Pierloot, E. Tsokos, L.G. Vanquickenborne, J. Phys. Chem. 100 (1996) 16545.
[40] C. Pollak, A. Rosa, E.J. Baerends, J. Am. Chem. Soc. 119 (1997) 7324.
[41] G.W. Tyndall, R.L. Jackson, J. Am. Chem. Soc. 109 (1987) 582.
[42] G.W. Tyndall, R.L. Jackson, J. Chem. Phys. 89 (1988) 1364.
[43] M. Protopapas, C.H. Keitel, P.L. Knight, Rep. Prog. Phys. 60 (1997) 389.
[44] W.C. Wiley, I.H. McLaren, Rev. Sci. Instrum. 26 (1955) 1150.
[45] B.R. Higginson, D.R. Lloyd, P. Burroughs, D.M. Gibson, A.F. Orchard, J. Chem. Soc., Faraday Trans. 2 69 (1973) 1659.
[46] F. Qi, X. Yang, S. Yang, H. Gao, L. Sheng, Y. Zhang, S. Yu, J. Chem. Phys. 107 (1997) 4911.
[47] T.R. Fletcher, R.N. Rosenfeld, J. Am. Chem. Soc. 110 (1988) 2097.
[48] B. Venkataraman, H. Hou, Z. Zhang, S. Chen, G. Bandukwalla, M. Vernon, J. Chem. Phys. 92 (1990) 5338.
[49] L. Bañares, T. Baumert, M. Bergt, B. Kiefer, G. Gerber, Chem. Phys. Lett. 267 (1997) 141.
[50] S.C. Yu, X. Xu, R. Lingle Jr., J.B. Hopkins, J.C. Hopkins, J. Am. Chem. Soc. 112 (1990) 3668.
[51] E.J. Heilweil, R.R. Cavanaugh, J.C. Stephenson, Chem. Phys. Lett. 134 (1997) 181.
[52] E.R. Bernstein, in: E.R. Bernstein (Ed.), Atomic and Molecular Clusters, Elsevier, Amsterdam, 1990, p.551.